Journal of Materials Chemistry C

Accepted Manuscript

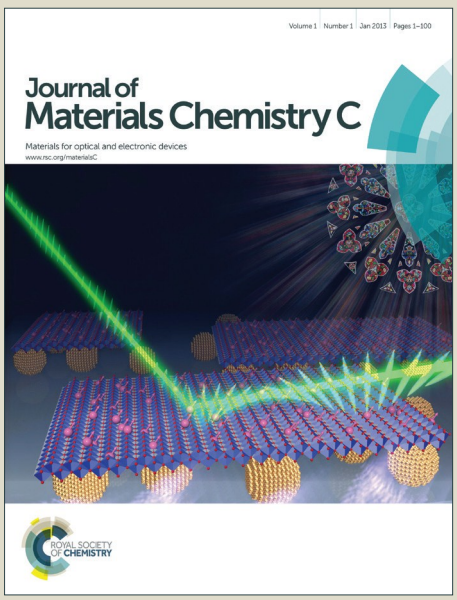

ROYAL SOCIETY OF CHEMISTRY

www.rsc.org/materialsC

Journal Name

ARTICLE

Non-resonant Raman Spectroscopy of Individual ZnO Nanowires via Au Nanorod Surface Plasmons

Received 00th January 20xx,
Accepted 00th January 20xx

DOI: 10.1039/x0xx00000x

www.rsc.org/

Andrea Pescaglini, [a] Eleonora Secco, [b] Alfonso Martin,[a] Davide Cammi,[c] Carsten Ronning, [c] Andrés Cantarero,[b] Nuria Garro[b] and Daniela Iacopino [a]

We present a non-resonant Raman spectroscopy study of individual ZnO nanowires mediated by Au nanorod surface plasmons. In this approach, selective excitation of the plasmonic oscillations with radiation energy below the semiconductor bandgap was used to probe surface optical modes of individual ZnO nanowires without simultaneous excitation of bulk phonons modes or band-edge photoluminescence. The development of a reproducible method for decoration of nanowires with colloidal Au nanorods allowed performing an extensive statistical analysis addressing the variability and reproducibility of the Raman features found in the hybrid nanostructures. An estimated field enhancement factor of 10^3 was calculated, which greatly exceeded previously reported values, and resulted in the detection of a surface optical mode not observable in bare ZnO nanowires under comparable experimental conditions. The role played by Au nanorods in the observed enhancement was investigated both theoretically and experimentally. Specifically, evidence of the superior capabilities in enhancing Raman signals of nanorod longitudinal surface plasmons compared to nanorod transversal surface plasmons is provided. Finite-difference-time domain (FDTD) simulations were used to support the experimental findings and corroborate the use of plasmonic resonances for spectroscopic investigation of individual semiconductor nanostructures.

Introduction

The superior sensitivity of surface-enhanced Raman spectroscopy (SERS) compared to traditional Raman spectroscopy has been extensively demonstrated in the past decades.[1] SERS exploits the intense electromagnetic fields generated by localized surface plasmons in noble metal nanostructures. This phenomenon compensates the weak nature of the inelastic photon-phonon scattering, thus overcoming the low detection sensitivity generally affecting Raman spectroscopy. The role played by plasmon resonances in SERS is two-fold: simultaneous amplification of the incident electromagnetic radiation and the radiation scattered off by the target object.[2, 3] This double process results in a 4-8 orders of magnitude enhancement of the Raman signal, achievable through an electric field amplification by a factor 10^2-10^4 generated in close proximity of the metal nanostructure.[4,5] For such reasons, SERS is particularly suitable for the investigation of molecular species that can be adsorbed on the surface of metal nanostructures.[6, 7] To date, low concentration detection of a vast range of molecules such as explosives,[8] pesticides,[9] drugs of abuse[10] and food contaminants[11, 12] has been demonstrated, as well as detection of chemical species down to single-molecule level.[13] In addition, also the investigation of nanostructured semiconductor surfaces can benefit from SERS.[14,15] Traditional Raman spectroscopy has been widely applied as non-destructive tool for the characterization of vibrational properties of both surface and core of semiconductor nanowires,[16, 17] therefore SERS technique has the potential to further extend these capabilities.

Enhanced Raman scattering has been observed in hybrid metal-semiconductor nanostructures under excitation with radiation energies corresponding to the localized surface plasmon resonance of the metal nanostructures. For example, Peng *et al.* reported a 7-fold Raman scattering enhancement of bulk modes of Si nanowires decorated with Ag nanoparticles.[18] A similar approach was used by Chen *et al.*,[19] who decorated Si nanowires with Au nanostructures of different morphologies demonstrating enhancement of the Si transverse optical phonon modes by a factor of 24 compared to the bare nanowires. In all these studies, the surface plasmon energies of the metal nanoparticles were close to the semiconductor band-gaps, therefore the conditions for SERS and for resonant Raman scattering (excitation energy equal or above the semiconductor band-gap) were simultaneously verified.

More intriguing is the possibility to investigate surface properties of hybrid semiconductor nanostructures using excitation energies below the semiconductor band-gap and

[a] Tyndall National Institute – University College Cork, Lee Maltings, Cork, Ireland
[b] Institute of Materials Science, University of Valencia, Valencia, Spain
[c] Institute of Solid State Physics, Friedrich-Schiller-University of Jena, Max-Wien-Platz 1, 07743 Jena, Germany

† Footnotes relating to the title and/or authors should appear here.
Electronic Supplementary Information (ESI) available: Optical properties of gold nanorods, detailed description of the fabrication methods used and statistical analysis of the Raman spectra. See DOI: 10.1039/x0xx00000x

corresponding to the plasmonic resonances of the metal components. This allows overcoming critical issues such as heating of the semiconductor material, its consequent degradation and the excitation of secondary emission, which could alter or hide targeted Raman signals.

However, the SERS approach for non-resonant Raman characterization of single nanowires has not been investigated so far. One of the key challenges in this field is the limited availability of reliable methodologies for the fabrication of hybrid metal nanoparticles-semiconductor nanowire nanostructures.[20] In fact, commonly used nanowire decoration techniques such as galvanic displacement,[21] photocatalytic reduction[22, 23] and sputtering,[6] suffer of poor control on the shape, size and distribution of plasmonic active metal components. For instance, reproducible and uniform incorporation of non-spherical metal nanoparticles into semiconductor nanowires has been scarcely pursued. As a result, Au nanorods-mediated Raman spectroscopy of semiconductor nanowires have been less investigated, despite the larger enhancing capabilities and higher optical tunability owned by metal nanorods compared to their spherical counterparts.[24, 25] Moreover, the small Raman scattering cross section generally hampers the spectroscopic investigation at single nanowire level and requires ensemble of nanowires to obtain detectable signals. This introduces a statistical broadening of the Raman features due to an average over many single nanowires. In contrast, spectral probing of hybrid structures under plasmon resonant conditions could potentially outclass the capabilities of traditional Raman spectroscopy, affording the investigation of individual nanostructures.

In this article we present a mask-selective droplet deposition method for the fabrication of hybrid Au nanorods–ZnO semiconductor nanowires with high yield and reproducibility. Plasmonic enhancement of ZnO surface optical modes was obtained on individual hybrid nanostructures under radiation energies below the semiconductor bandgap and corresponding to the nanorod plasmon resonance. In comparison, no enhancement was detected during investigation of bare single ZnO nanowires. Detailed theoretical and experimental investigation of the enhancement process demonstrated the plasmonic origin of the enhancement process driven by the longitudinal surface plasmon resonance mode of Au nanorods deposited on ZnO nanowires.

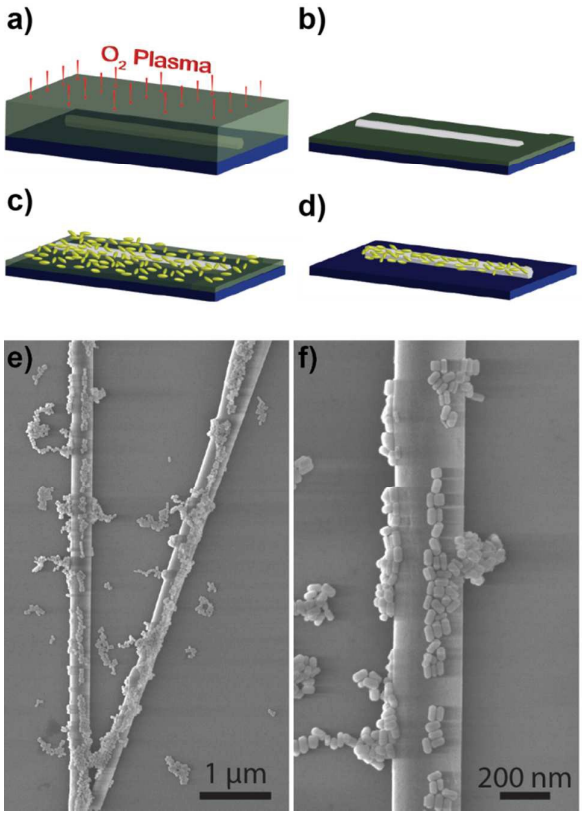

Figure 1. Schematic drawing of the mask-selective droplet deposition method. a) ZnO nanowires deposited on Si/SiO_2 substrate covered with spin coated polymer resist; b) polymer resist etched by O_2 plasma; c) Au nanorod solution deposited on the entire substrate and dried; d) removal of residual resist layer by solvent cleaning; e-f) Representative low and high magnification SEM images of hybrid nanostructures obtained by mask-selective droplet deposition method.

Results and discussion

Colloidal Au nanorods used in this work were synthesized by a seed-mediated method reported by Puebla *et al.*[26] Nanorods were characterized by a mean diameter and length of 29 ± 5 nm and 68 ± 5 nm, respectively, and showed a transversal plasmon resonance (TPR) centered at 524 nm and longitudinal plasmon resonance (LPR) centered at 657 nm (see ESI, figure S1). Au nanorods were stabilized in solution by hexadecyltrimethylammonium bromide (CTAB) molecules, which form a 2-3 nm thick layer around the nanorod metallic core.[27] ZnO nanostructures with mean lengths of 5 ± 2 μm and diameters of 150 ± 46 nm were grown by a simple vapor transport technique enabled by the vapor-liquid-solid (VLS) mechanism, as reported elsewhere.[28] In order to deposit nanorods on the surface of ZnO nanowires a *mask-selective droplet deposition* was developed, as schematically depicted in Figure 1a-d.

Firstly, ZnO nanowires were mechanically dispersed on a Si/SiO_2(300 nm) substrate and covered with 1.4 μm of photoresist (S1813) by spin-coating (Figure 1a). Subsequently, the photoresist was etched by an O_2-plasma. A constant etching rate of ~250 nm/min was used to reduce the photoresist thickness down to ~ 150 nm, which exposed only the nanowire top surface while leaving the majority of its surface embedded in the photoresist (Figure 1b). A droplet of the Au nanorod aqueous solution was deposited over the substrate and evaporated at 110 ºC resulting in homogeneous distribution of nanorods both on the nanowire top surface and on the area covered by the photoresist (Figure 1c). The residual photoresist along with the nanorods deposited on its surface was then removed by solvent cleaning (Figure 1d). Representative SEM images of the final Au nanorods-decorated ZnO nanowire hybrid nanostructures are shown in Figure 1e-f depicting high yield deposition of nanorods preferentially located on the nanowire surfaces. In contrast, direct droplet deposition of the nanorod suspension on substrate-deposited nanowires led to accumulation of nanorods on the substrate surface adjacent to the nanowires (see ESI, Figure S2). Therefore the strict control of photoresist thickness in the mask-selective method resulted in a more effective decoration of the nanowire surface. Moreover, homogeneous and controlled photoresist etching by O_2-plasma was achieved over the entire substrate, leading to large yield of decorated nanowires per sample.

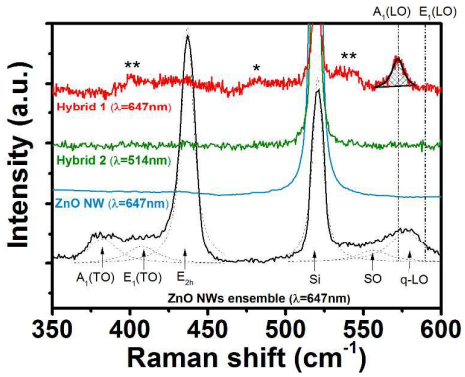

Figure 2. Representative Raman spectra of an ensemble of ZnO nanowires recorded at 647 nm (black curve) with the corresponding fits of the observed Raman modes (dotted lines); single bare ZnO nanowire recorded at 647 nm (blue curve); single hybrid nanostructure at 514 nm (green curve); and 647 nm (red curve); all spectra were recorded with a laser excitation power of 0.5 mW. The spectra of the hybrid nanowire (green and red curves) appeared over an intense background, which has been subtracted. In the hybrid nanostructure spectrum the SO mode is shadowed in grey, the single asterisk indicate the peaks associated to crystalline CTAB and the double asterisk those associated to bare Au nanorods deposited on Si/SiO_2 substrate.

Figure 2 (black curve) shows the Raman spectrum of a disordered ensemble of as-grown ZnO nanowires on a Si/SiO_2 substrate illuminated with an excitation wavelength of 647 nm. The random orientation of the nanowires with respect to the propagation of the excitation beam allows the simultaneous observation of all optical phonons. Thus, besides the Raman line of the Si substrate at 519 cm^{-1}, an intense sharp peak is observed at 438 cm^{-1} corresponding to the E_{2h} mode of ZnO. The contribution of other optical phonons is also resolved by fitting the spectrum with several Lorentzian peaks: the A_1(TO) at 378 cm^{-1}, the E_1(TO) at 410 cm^{-1}, and the quasi-LO at 577 cm^{-1} (resulting from the mixture of the A_1(LO) and E_1(LO) modes). The latter peak presents an asymmetry at the low frequency side, which is compatible with a surface optical (SO) mode centered at 554 cm^{-1}. SO phonons have frequencies lying in between those of the TO and the LO bulk modes and have been reported in the 545-565 cm^{-1} frequency range for ZnO nanoparticles.[29]

The featureless blue line in Figure 2 represents the Raman spectrum collected from an individual ZnO nanowire deposited on Si/SiO_2 substrate under illumination at 647 nm. The excitation light propagates perpendicular to the nanowire axis (z-direction) in this experiment. Although several modes are allowed by the Raman scattering selection rules for this backscattering geometry (A_1(TO), E_1(TO) and E_{2h}), no modes were observed due to the small cross-section of the non-resonant Raman scattering process for which the generation of detectable signals requires probing of large nanowire densities.

In contrast, the Raman spectrum of an individual hybrid nanostructure (red line in Figure 2) recorded with a wavelength of 647 nm presents multiple features over an intense background. It shows an intense peak centered at 572 cm^{-1}, which is compatible with a SO mode for ZnO nanowire as will be discussed in detail below. An additional peak appears centered at 480 cm^{-1} (pointed with a single asterisk in Figure 2), characteristic of crystalline CTAB used as stabilizing agent during nanorod synthesis.[30, 31] Furthermore, peaks at 401 and 544 cm^{-1} (double asterisk in Figure 2) can be attributed to CTAB vibrational transitions, as they were also found in Raman spectra of dense Au nanorod ensembles (see ESI, figure S3). The generation of these peaks was likely a result of electromagnetic SERS enhancement occurring between closely-spaced nanorods, which altered the CTAB molecular vibrational resonances[15] introducing additional modes compared to the unbound molecules.[32]

Since different hybrid structures presented slightly different spectroscopic features (see ESI, figure S4) a careful and systematic statistical analysis was carried out in order to classify the observed peaks. To this aim, two hybrid nanostructure samples, namely A and B, were used. Hybrid nanostructures A were fabricated following the deposition process described in Figure 1a-d. However, since the exposure to O_2-plasma can potentially damage the nanowire surface, affecting the frequency position of the SO mode, additional hybrid nanostructures B were fabricated substituting the plasma etching step (Figure 1b) with an alternative lithographic process previously developed (see ESI).[33] Figure 3 presents the statistical analysis obtained with data collected

from hybrids A and hybrids B. The y-axis reports the frequency-weighted intensity (FWI) of measured Raman peaks calculated multiplying the average measured intensity of the peak by its occurrence. For simplicity peaks already attributed to crystalline CTAB and those also appearing for Au nanorod ensemble samples were omitted (see ESI, figure S5). The graphic shows that the SO mode at 572 cm^{-1} was the most relevant peak for both samples. Additional modes centered at 382 cm^{-1}, 422 cm^{-1}, 510 cm^{-1} and 554 cm^{-1} for hybrid A and at 382 $cm^{-1}$and 555 cm^{-1} for hybrid B were also detected. Although these modes cannot be unequivocally assessed, we hypothesize that they could be associated to SERS chemical enhancement processes occurring by charge transfer between CTAB molecules and ZnO.[34]

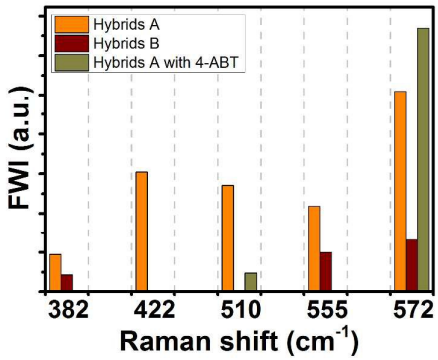

Figure 3. Frequency-weighted intensity of Raman peaks in hybrids A (orange histogram), hybrids B (brown histogram) and hybrids A after immersion in 4-ABT (green histogram). The peaks observed in the CTAB crystalline or in Au nanorods deposited on Si/SiO_2 substrate were omitted.

In order to complete the spectral assignation and disregard completely peaks originating from CTAB, hybrids A were immersed in a methanol solution (1 mM) of 4-aminobenzenethiol (4-ABT) in order to replace CTAB molecules adsorbed on nanorod surfaces. 4-ABT has been largely used as model molecule for SERS, due to its peculiar and well characterized Raman features.[24] The Raman spectrum of hybrids A after immersion in 4-ABT showed the distinctive 4-ABT Raman modes at 1004, 1073, 1139 and 1187 cm^{-1}, demonstrating the effective attachment of the molecule to the nanorod surfaces (see ESI, Figure S6). Statistical analysis performed on hybrid A following immersion in 4-ABT (Figure 3) showed occurrence of only two peaks previously detected (510 and 572 cm^{-1}), confirming the CTAB origin of the remaining features (see ESI, Figure S7). Overall, only the peak at 572 cm^{-1} was detected with comparable intensity in the three samples analyzed, and therefore it was attributed to a mode originating from the ZnO nanowires.

The unequivocal attribution of the observed mode requires revisiting the Raman selection rules under the current experimental geometry. Considering the random orientation of the Au nanorods with respect to the c-axis of the ZnO nanowire, the electromagnetic field generated by the plasmonic oscillations propagates perpendicular to the nanowire axis with a random polarization. Thus, four bulk modes (A_1(TO), E_1(TO), E_1(LO), and E_{2h}) would be allowed in this configuration. If the 572 cm^{-1} peak corresponded to a bulk mode, it would be accompanied by other bulk modes. Instead, the 572 cm^{-1} peak appeared as an isolated feature, thus ruling out the possibility of its bulk origin. This is also in agreement with the short penetration of the plasmonic fields, as will be discussed in detail in Figure 4. The frequency of the SO mode in the hybrid nanowires appears blue-shifted with respect to that of ZnO nanowire ensemble (see red and black curves in Figure 2) and the values reported in the literature.[35] One possible explanation of the observed frequency shift could be the effect of the SiO_2 substrate. Assuming an infinite long cylindrical wire, the dispersion relation $\omega_{SO}(q)$ for a SO mode in the limit where the phonon wavevector q and the nanowire radius r satisfies the condition qr>>1, can be written as[36-38]

$$\omega_{SO}^2 = \omega_{TO}^2 \frac{\varepsilon_0 + \varepsilon_m}{\varepsilon_\infty + \varepsilon_m} \quad (1)$$

where ω_{TO} is the TO mode frequency at zone center, ε_0 = 10.29 and ε_∞=4.47 are the static and high-frequency dielectric constant of the bulk ZnO respectively and ε_m the dielectric constant of the surrounding medium. Since the nanowire radius r is ~150 nm and the SO phonon wavevector is on the order of 10^7-10^9 m^{-1},[39] the condition qr>>1 is verified. The dielectric constant ε_m should be estimated averaging among the dielectric constants of the different surrounding media.[16, 40] In the case of a dense ensemble of nanowires, where a mixed composition of air and ZnO (ε=3.9) surrounds a single nanowire, ε_m is 2.45, whereas for the hybrid individual nanowires the SiO_2 substrate (ε=2.37) and air gives ε_m= 1.7. It is therefore expected that the SO mode of the hybrid wire blue-shifts around 20 cm^{-1}.

The results shown in Figure 3 demonstrate a selective and reproducible enhancement of the ZnO SO mode in hybrid nanostructures under excitation at 647 nm, in resonance with the longitudinal plasmon resonance (LPR) of the Au nanorod components. Remarkably, Figure 2 (green line) shows that no measurable enhancement was detected in the Raman spectra of individual hybrid structures for an excitation wavelength of 514 nm, in resonance with the Au nanorod transversal plasmon resonance (TPR). In order to clarify this point, finite-difference time–domain (FDTD) simulations were performed on a system constituted by an Au nanorod (29 x 68 nm) in contact with a ZnO surface. A 3 nm organic shell (refractive index, n = 1.4) representing the CTAB layer around the Au nanorod was also added to the calculations.[41, 42] Figure 4a shows the simulated scattering spectra calculated with light propagating along the y-direction and polarized along the nanorod z- (longitudinal direction) and x-axis (transversal direction), respectively.

Journal Name

ARTICLE

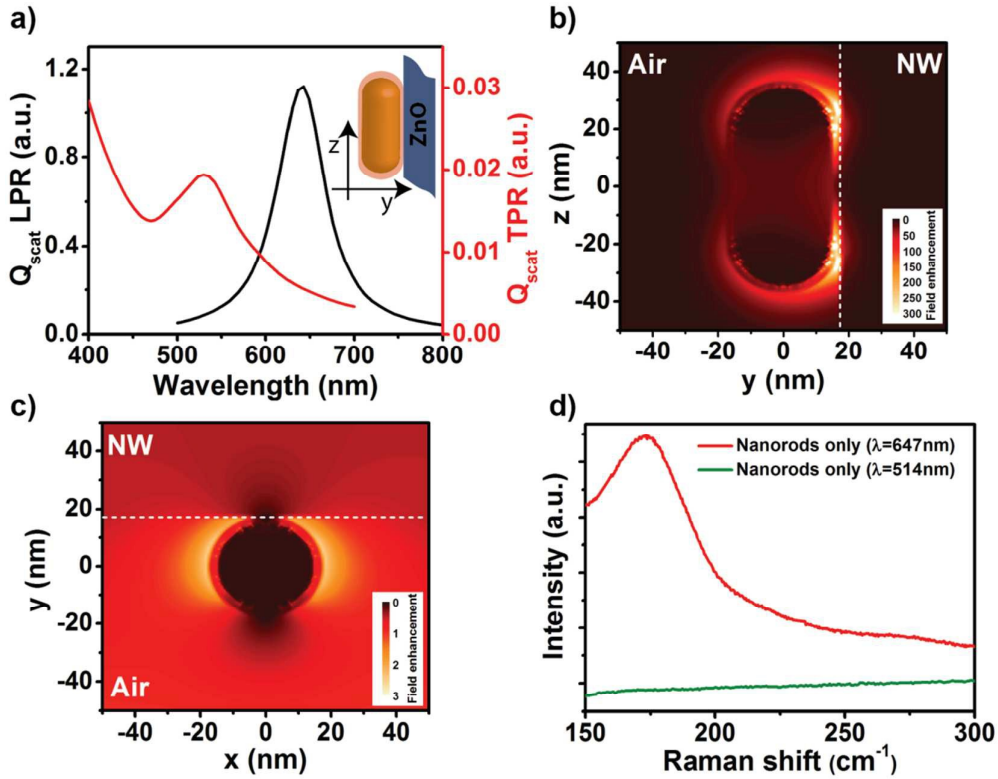

Figure 4. a) FDTD simulation of the scattering cross section normalized to the geometrical cross section of a Au nanorod 29x68 nm on a ZnO nanowire under light polarized along –z (black curve) and -x (red curve) and light propagating along -y. Inset: schematic of the simulated Au nanorod-ZnO nanowire hybrid structure; b-c) FDTD simulation of the electric field enhancement factor for light polarized along z-axis and x-axis, respectively; d) Raman spectra of Au nanorod ensemble measured at 647 nm (red curve) and 514 nm (green curve).

The LPR and TPR maxima were calculated at 642 nm and 529 nm, in reasonable agreement with the experimental values (compare with ESI, Figure S1). Figure 4b shows that longitudinal excitation generates a field enhancement factor β_{EF} larger than 300, concentrated in the space between nanorod and nanowire; β_{EF} is defined as = $|E_{scat}|^2/|E_{inc}|^2$, with E_{scat} and E_{inc} corresponding to the scattered and incident electric field intensity, respectively. However, β_{EF} calculated inside the nanowire in proximity of the surface was around ~70 and rapidly decreased to unity within 20 nm distance from the surface, supporting the superficial nature of the detected ZnO mode. On the other hand, transversal excitation (Figure 4c) generated a β_{EF} of ~3 at the metal surface, that barely penetrates the semiconductor surface. The negligible field enhancement under excitation of the TPR compared to the two orders of magnitude generated by LPR provides a reasonable explanation for the absence of Raman features in the experimental spectra recorded at 514 nm, compared to the spectra measured at 647 nm excitation wavelength (Figure 2, red and green curves). As further evidence, Figure 4d reports the experimental SERS spectra of dense Au nanorod ensemble measured at 647 nm and 514 nm. The spectroscopic response at 174 cm^{-1} originated from the Br-Au bond of the CTAB molecules adsorbed on the Au nanorods surface was used as reference to compare the strength of SERS in both cases.[43] According to the larger field enhancement calculated for longitudinal excitation, the SERS spectrum of Figure 4d showed an intense Br-Au peak for excitation at 647 nm, whereas no features were observed for excitation at 514 nm.

The enhancement of the SO mode in the hybrid nanostructure resulted to be at least a factor 10^3, and was estimated by dividing the Raman intensity at 572 cm^{-1} of the hybrid structure by the background intensity of the bare ZnO nanowire. Within the $|E|^4$-approximation,[3] the Raman

enhancement factor (EF) is proportional to the β_{EF}^2 inside the nanowire. Using β_{EF} ~70 calculated by FDTD simulations, the resulting EF value was found of the order of 10^3, in excellent agreement with the experimental results. However, the EF value reported is several orders of magnitude smaller than the EF found in SERS experiments on molecules adsorbed on metal nanostructures.[13] This is a natural consequence of the fast decay of the electromagnetic field intensity outside the metal surface, which limits the volume of the semiconductor within the plasmonic enhancement range as well as the β_{EF} values inside the nanowire. For this reason, despite the proved advantages offered by this approach for surface Raman investigation of single semiconductor nanostructures, further optimization is still required in order to improve the reproducibility and the stability of this approach. Additionally, improvements in nanorod distribution along the nanowire surface (in terms of density and location) could lead to an increase of the signal intensity that is expected to scale up proportional to the number of deposited nanorods.

Conclusions

In conclusion, we investigated the plasmonic-enhanced non-resonant Raman scattering of surface optical modes in individual gold nanorods-ZnO nanowire hybrid systems. The large energy separation between the semiconductor band-edge absorption (3.3 eV) and the nanoparticle plasmon energies (~2 eV) allowed to perform a selective probing of the Raman scattering mediated by the plasmonic resonances without any detectable contribution from the semiconductor material. The results were supported by extensive statistical analysis of the detected Raman features, which included a careful investigation of the variability of the SERS peaks introduced by the organic layer on the colloidal nanorods, and allowed to assess the reproducibility of the presented approach. In addition, the key role played by the longitudinal plasmon mode in the enhancement process was experimentally and theoretically demonstrated and corroborates the use of rod-shaped nanoparticles instead of the more frequently used spherical nanoparticles. This study opens up new possibilities for the spectroscopic characterization of surface properties of semiconductor nanowires and related heterostructures that, due to their large surface-to-volume ratio, could provide meaningful insights on the optical and electrical properties of nanowire-based devices. Furthermore, the results presented in this work reinforce the increasing interest in 1D semiconductor-metal nanostructure hybrid devices and contribute to the understanding and development of their enhanced and engineered properties relevant for optoelectronic and sensing applications.

Methods

Growth of ZnO nanowires. ZnO nanostructures were grown by chemical vapor deposition (CVD) using vapour-liquid-solid (VLS) mechanism in a high temperature tube furnace.[28] Briefly, ZnO powder was placed in the middle part of a tube furnace and heated up at 1350 ºC. Silicon substrates with a nominal 10 nm thick Au coating were located downstream in the colder region of the tube furnace at around 1050 ºC. The transport of evaporated ZnO material was favored by 50 sccm Ar gas flow at constant pressure of 100 mbar. The growth time was 60 minutes.

Synthesis of Au nanorods. Au nanorods were synthesized using a seed-mediated method described by Puebla *et al*.[26] The as prepared Au nanorod solution (1 mL) was centrifuged twice to remove CTAB excess and re-dispersed in 1 mL of deionizied water with resistivity equal to 18 MΩ cm. The final CTAB concentration was estimated to be 0.05 mM.

Fabrication of Au nanorods- ZnO nanowire hybrid structures. ZnO nanowires were mechanically transferred on a clean $Si(n^{++})/SiO_2$ (300nm) substrate and covered by a layer of photoresist (S1813) by spin-coating. The photoresist was firstly baked at 120 ºC for 2 min and subsequently exposed to a 50 sccm flow of O_2-Plasma (RIE system, 100 W, 45 mTorr, 7 min). The exposure to plasma was regulated in order to reduce the photoresist thickness below the ZnO nanowire thickness (~150 nm) and to leave only the nanowire top surface exposed. 5 μL of Au nanorod aqueous solution were dropped on the Si substrate and dried at constant temperature of 110 ºC. Residual photoresist containing nanorods deposited on the substrate and not attached to the nanowire surface was removed by standard solvent cleaning.

FDTD simulations. 3D FDTD simulations were performed using the commercial available software LUMERICAL FDTD Solutions. In the simulations the Au nanorod had a cylindrical body of 29 nm in diameter ending with two hemispherical caps with a total length of 68 nm surrounded by 3 nm of dielectric layer with refractive index n=1.4. The ZnO nanowire was approximated with a cylinder having 200 nm in diameter and 500 nm in length with a refractive index of n=1.98. The refractive index of air was assumed to be n=1 and the polymer resist n=1.61.

Morphological characterization. SEM measurements were performed using a JSM 7500F, JEOL UK Scanning Electron Microscope at operating voltages of 10 kV.

Raman spectroscopy. All Raman measurements were carried on in back-scattering configuration (i.e. wave vectors of the incident and the scattered light parallel). A microscope objective (100 X) was used to focus the laser on the sample with a spot diameter of 1μm. The microscope was coupled to a T64000 triple spectrometer from Jobin-Yvon® and a nitrogen-cooled charge-coupled device detector. The spectral resolution of the entire system was of 1 cm^{-1} at 500 nm. Substitution of CTAB with 4-ABT molecules was obtained by sample immersion for 6 h in a methanol solution of 4-ABT 1 mM.

Acknowledgements

This work was supported by the European Commission under the Marie Curie ITN project "Nanowiring" (265073), FP7 NMP project "Hysens" (263091), Science Foundation Ireland under the Research Frontiers Programme (SFI/09RFP/CAP2455) and the Irish Higher Education Authority PRTLI programs (Cycle 3 "Nanoscience" and Cycle 4 "INSPIRE").

Notes and references

1 Z.-Q. Tian, B. Ren, J.-F. Li and Z.-L. Yang, *Chem. Commun.*, 2007, DOI: 10.1039/B616986D, 3514-3534.

2 P. Alonso-González, P. Albella, M. Schnell, J. Chen, F. Huth, A. García-Etxarri, F. Casanova, F. Golmar, L. Arzubiaga, L. E. Hueso, J. Aizpurua and R. Hillenbrand, *Nat Commun*, 2012, **3**, 684.

3 E. C. Le Ru and P. G. Etchegoin, *MRS Bulletin*, 2013, **38**, 631-640.

4 C. Noguez, *J. Phys. Chem. C*, 2007, **111**, 3806-3819.

5 H. Cang, A. Labno, C. Lu, X. Yin, M. Liu, C. Gladden, Y. Liu and X. Zhang, *Nature*, 2011, **469**, 385-388.

6 S. Deng, H. M. Fan, X. Zhang, K. P. Loh, C. L. Cheng, C. H. Sow and Y. L. Foo, *Nanotechnology*, 2009, **20**, 175705.

7 C. Cheng, B. Yan, S. M. Wong, X. Li, W. Zhou, T. Yu, Z. Shen, H. Yu and H. J. Fan, *ACS Applied Materials & Interfaces*, 2010, **2**, 1824-1828.

8 M. K. Khaing Oo, C.-F. Chang, Y. Sun and X. Fan, *Analyst*, 2011, **136**, 2811-2817.

9 Y. Zhang, Z. Wang, L. Wu, Y. Pei, P. Chen and Y. Cui, *Analyst*, 2014, **139**, 5148-5154.

10 M. Sanles-Sobrido, L. Rodriguez-Lorenzo, S. Lorenzo-Abalde, A. Gonzalez-Fernandez, M. A. Correa-Duarte, R. A. Alvarez-Puebla and L. M. Liz-Marzan, *Nanoscale*, 2009, **1**, 153-158.

11 A. Martin, J. J. Wang and D. Iacopino, *RSC Advances*, 2014, **4**, 20038-20043.

12 H. W. Kang, J. Leem and H. J. Sung, *RSC Advances*, 2015, **5**, 51-57.

13 R. F. Aroca, *Phys. Chem. Chem. Phys.*, 2013, **15**, 5355-5363.

14 G. Shan, L. Xu, G. Wang and Y. Liu, *J. Phys. Chem. C*, 2007, **111**, 3290-3293.

15 J. F. Li, Y. F. Huang, Y. Ding, Z. L. Yang, S. B. Li, X. S. Zhou, F. R. Fan, W. Zhang, Z. Y. Zhou, Y. WuDe, B. Ren, Z. L. Wang and Z. Q. Tian, *Nature*, 2010, **464**, 392-395.

16 A. Cros, *physica status solidi (RRL) – Rapid Research Letters*, 2013, **7**, 727-738.

17 M. Gómez-Gómez, N. Garro, J. Segura-Ruiz, G. Martinez-Criado, A. Cantarero, H. T. Mengistu, A. García-Cristóbal, S. Murcia-Mascarós, C. Denker, J. Malindretos and A. Rizzi, *Nanotechnology*, 2014, **25**, 075705.

18 Z. Peng, H. Hu, M. I. B. Utama, L. M. Wong, K. Ghosh, R. Chen, S. Wang, Z. Shen and Q. Xiong, *Nano Lett.*, 2010, **10**, 3940-3947.

19 R. Chen, D. Li, H. Hu, Y. Zhao, Y. Wang, N. Wong, S. Wang, Y. Zhang, J. Hu, Z. Shen and Q. Xiong, *J. Phys. Chem. C*, 2012, **116**, 4416-4422.

20 A. Pescaglini and D. Iacopino, *J. Mater. Chem. C*, 2015, **3**, 11785-11800.

21 S. Y. Sayed, F. Wang, M. Malac, A. Meldrum, R. F. Egerton and J. M. Buriak, *ACS Nano*, 2009, **3**, 2809-2817.

22 I. C. Chen, Y.-C. M. Liou, J. Yang and T.-Y. Shieh, *J. Raman Spectrosc.*, 2011, **42**, 339-344.

23 E. Satheeshkumar and J. Yang, *J. Raman Spectrosc.*, 2014, **45**, 407-413.

24 A. Martín, A. Pescaglini, C. Schopf, V. Scardaci, R. Coull, L. Byrne and D. Iacopino, *J. Phys. Chem. C*, 2014, **118**, 13260-13267.

25 S. T. Sivapalan, B. M. DeVetter, T. K. Yang, T. van Dijk, M. V. Schulmerich, P. S. Carney, R. Bhargava and C. J. Murphy, *ACS Nano*, 2013, **7**, 2099-2105.

26 R. A. Alvarez-Puebla, A. Agarwal, P. Manna, B. P. Khanal, P. Aldeanueva-Potel, E. Carbó-Argibay, N. Pazos-Pérez, L. Vigderman, E. R. Zubarev and N. A. Kotov, *Proceedings of the National Academy of Sciences*, 2011, **108**, 8157-8161.

27 B. Nikoobakht and M. A. El-Sayed, *Langmuir*, 2001, **17**, 6368-6374.

28 C. Borchers, S. Müller, D. Stichtenoth, D. Schwen and C. Ronning, *J. Phys. Chem. B*, 2006, **110**, 1656-1660.

29 H. Zeng, W. Cai, B. Cao, J. Hu, Y. Li and P. Liu, *Appl. Phys. Lett.*, 2006, **88**, 181905.

30 K. Kalyanasundaram and J. K. Thomas, *The Journal of Physical Chemistry*, 1976, **80**, 1462-1473.

31 B. Bozzini, L. D'Urzo, M. Re and F. Riccardis, *J. Appl. Electrochem.*, 2008, **38**, 1561-1569.

32 C. Yu, L. Varghese and J. Irudayaraj, *Langmuir*, 2007, **23**, 9114 - 9119.

33 A. Pescaglini, A. Martín, D. Cammi, G. Juska, C. Ronning, E. Pelucchi and D. Iacopino, *Nano Lett.*, 2014, DOI: 10.1021/nl5024854.

34 K. Kim, K. L. Kim and K. S. Shin, *Phys. Chem. Chem. Phys.*, 2013, **15**, 9288-9294.

35 H. Zeng, W. Cai, B. Cao, J. Hu, Y. Li and P. Liu, *Appl. Phys. Lett.*, 2006, **88**, -.

36 Q. Xiong, J. Wang, O. Reese, L. C. Lew Yan Voon and P. C. Eklund, *Nano Lett.*, 2004, **4**, 1991-1996.

37 A. R. Bhatt, K. W. Kim, M. A. Stroscio, G. J. Iafrate, M. Dutta, H. L. Grubin, R. Haque and X. T. Zhu, *J. Appl. Phys.*, 1993, **73**, 2338-2342.

38 M. A. Stroscio, K. W. Kim, M. A. Littlejohn and H. Chuang, *Phys. Rev. B*, 1990, **42**, 1488-1491.

39 R. Gupta, Q. Xiong, G. D. Mahan and P. C. Eklund, *Nano Lett.*, 2003, **3**, 1745-1750.

40 C. Novo, A. M. Funston, I. Pastoriza-Santos, L. M. Liz-Marzan and P. Mulvaney, *J. Phys. Chem. C*, 2007, **112**, 3-7.

41 T. K. Sau and C. J. Murphy, *Langmuir*, 2005, **21**, 2923-2929.

42 C. Yu, L. Varghese and J. Irudayaraj, *Langmuir*, 2007, **23**, 9114-9119.

43 B. Nikoobakht, J. P. Wang and M. A. El-Sayed, *Chem. Phys. Lett.*, 2002, **366**, 17-23.

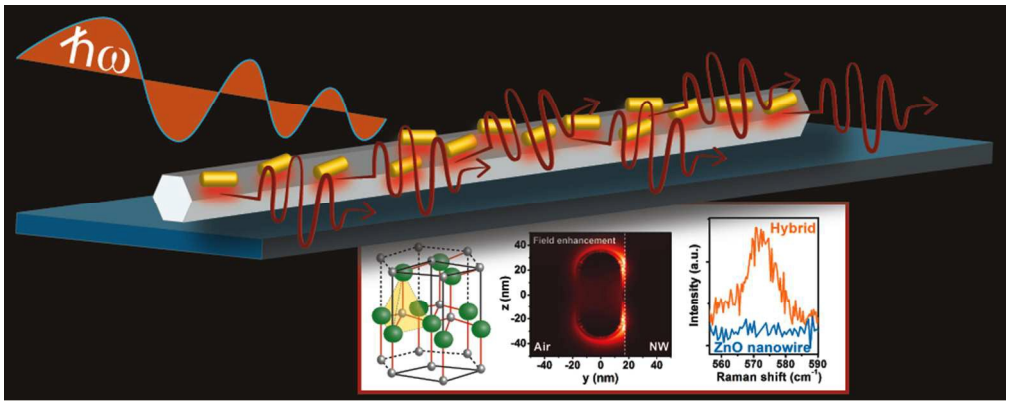

87x34mm (300 x 300 DPI)